THE ASTROPHYSICAL JOURNAL, 504:671–679, 1998 September 10

OPTICAL VARIABILITY IN ACTIVE GALACTIC NUCLEI: STARBURSTS OR DISK INSTABILITIES?

T. KAWAGUCHI AND S. MINESHIGE
Department of Astronomy, Kyoto University, Sakyo-ku, Kyoto 606-8502, Japan; kawaguti@kusastro.kyoto-u.ac.jp, minesige@kusastro.kyoto-u.ac.jp
M. UMEMURA
Center for Computational Physics, University of Tsukuba, Tsukuba, Ibaraki 305-0006, Japan; umemura@rccp.tsukuba-u.ac.jp
AND
EDWIN L. TURNER
Princeton University Observatory, Peyton Hall, Princeton, NJ 08544; elt@astro.princeton.edu
Received 1997 November 20; accepted 1998 April 17

ABSTRACT

Aperiodic optical variability is a common property of active galactic nuclei (AGNs), though its physical origin is still open to question. To study the origin of the optical-ultraviolet variability in AGNs, we compare light curves of two models to observations of quasar 0957+561 in terms of a structure function analysis. In the starburst (SB) model, random superposition of supernovae in the nuclear starburst region produces aperiodic luminosity variations, while in the disk-instability (DI) model, variability is caused by instabilities in the accretion disk around a supermassive black hole. We calculate fluctuating light curves and structure functions, $V(\tau)$, by simple Monte Carlo simulations on the basis of the two models. Each resultant $V(\tau)$ possesses a power-law portion, $[V(\tau)]^{1/2} \propto \tau^{\beta}$, at short time lags ($\tau$). The two models can be distinguished by the logarithmic slope β; $\beta \sim 0.74$–0.90 in the SB model and $\beta \sim 0.41$–0.49 in the DI model, while the observed light curves exhibit $\beta \sim 0.35$. Therefore, we conclude that the DI model is favored over the SB model in explaining the slopes of the observational structure function in the case of 0957+561, though this object is a radio-loud object and thus is not really a fair test for the SB model. In addition, we examine the time asymmetry of the light curves by calculating $V(\tau)$ separately for the brightening and the decaying phases. The two models exhibit opposite trends of time asymmetry to some extent, although the present observation is not long enough to test this prediction.

Subject headings: accretion, accretion disks — galaxies: active — galaxies: nuclei — instabilities

1. INTRODUCTION

Emission from active galactic nuclei (AGNs) has long been known to exhibit rapid and apparently random variability, over wide wavelength ranges from radio to X-ray or γ-ray (Krolik et al. 1991; Edelson et al. 1996). The fluctuation power spectrum has a power-law dependence on frequency, $\propto f^{-\alpha}$ with $\alpha \sim 1.0$–2.5 (Lawrence & Papadakis 1993; Green, McHardy, & Lehto 1993; Leighly & O'Brien 1997; Hayashida et al. 1998). Simultaneous multiwavelength observations have also revealed that there is strong time correlation between optical-ultraviolet (UV) and X-ray emission with little delay (Clavel et al. 1992; Edelson et al. 1996; Warwick et al. 1996), while the variation of the Hβ emission line follows the optical continuum variation with a delay of $\sim$20 days (Peterson et al. 1994; see Netzer & Peterson 1997 for emission-line variability). At present, many multiwavelength monitoring projects are in progress (see, e.g., Kundić et al. 1997; O'Brien & Leighly 1997, and references therein). In spite of these successful observations, the location of regions emitting in various energy bands and the physical origin of the variability are still open to question. In addition, the apparent time reversibility of AGN light curves has been recognized as a potential problem recently (Aretxaga 1997). Therefore, one of the major goals of variability studies is to identify and characterize the physical processes responsible for the observed variability.

The presence of huge energy outputs and high-energy emission strongly indicates the existence of a supermassive black hole and a surrounding accretion disks in an AGN (see, e.g., Rees 1984). This picture is supported by a number of observations; e.g., the detection of a large peculiar-velocity dispersion of stars near the nucleus, substantial short-term X-ray variability, and asymmetric broad Fe fluorescence line features (Tanaka et al. 1995). Moreover, it has been suggested that the optical-ultraviolet emission may come mainly from the accretion disk, which is supported indirectly by the rough agreement between the theoretical spectral energy distribution (SED) calculated by the standard accretion disk model and observational SEDs (Shields 1978; Malkan 1983). However, since the standard optically thick accretion disk is too cool to produce any X-ray emission, another mechanism is required. Regarding the relation between these two energy sources, there is the following suggestion. The absence of time lag between the UV and the X-ray variability suggests reprocessing; the UV emission comes from the optically thick disk, which is partially illuminated by an X-ray source (i.e., an accretion disk atmosphere) and is also heated by internal viscosity and accretion (Santos-Lleó et al. 1995; Edelson et al. 1996). Occasional flare events or blob formation caused by some instability in the atmosphere should produce a luminosity variation in time. This is the basic idea behind the disk-instability (DI) model.

There exist, however, completely different models for radio-quiet AGNs, which do not always involve black holes. The most popular among them is the starburst (SB) model (see, e.g., Terlevich et al. 1992). In this model, the energy is generated by violent star formation activity in the innermost regions of AGNs. The observed flux variability of AGNs is ascribed to transient phenomena associated with the evolution of massive stars and supernovae (SNe). There

is no difficulty in accounting for the average bolometric luminosity of AGNs in terms of SNe; for example, a Seyfert galaxy luminosity of 10^{44} ergs s^{-1} can be accommodated by about one SN per year (the energy released by one supernova being $\sim 10^{51}$ ergs), whereas a high-luminosity QSO would require a few hundred SNe per year. However, it would appear to be difficult to explain the rapid X-ray variability with the SB model.

To answer these questions, we have analyzed the optical variability of quasar 0957+561 and each of the SB and DI models, using a first-order structure function analysis. The main goal of the present study is to clarify distinction between variability caused by starburst (SB) and disk instability (DI) and consequently to derive some constraints on plausible models. Structure function analysis provides a method of quantifying time variability without the problems of windowing, aliasing, etc., that are encountered in the traditional Fourier analysis technique. It potentially provides good information on the nature of the process that causes variation. This technique has been used previously by a number of authors for the study of time series (see, e.g., Simonetti, Cordes, & Heeschen 1985; Hughes, Aller, & Aller 1992; Press, Rybicki, & Hewitt 1992).

The best available QSO optical light curve, in terms of sampling rate, data volume, and photometric accuracy, was obtained by Kundić et al. (1995, 1997) for the gravitational lens system 0957+561A/B. The data were obtained for the purpose of determining the lensing differential time delay between the two images of the background quasar, a measurement that had generated considerable controversy over the years (see Haarsma et al. 1997). The clear determination of the delay (Kundić et al. 1997), which effectively ended the controversy, makes the system even more suitable for our purposes since the light curves of the two images can now be combined to produce one effectively even longer and better-sampled light curve of the source itself. Moreover, comparison of the light curves of the two images allows variations intrinsic to the source (in which we are interested) to be distinguished from those produced by any process occurring along the line of sight (such as microlensing or extinction variations with time, in which we are not interested). In other words, variations intrinsic to the source will occur in both images, though delayed in image B relative to A, while those which are extrinsic will be seen in only one image. This technique indicates that the observed variations are entirely, or almost entirely, due to intrinsic source variations and that any extrinsic variations have photometric amplitudes no larger than a few hundredths of a magnitude, comparable to the photometric noise. Finally, the fact that gravitational lensing occurs because of random chance alignments of foreground and background objects implies that there is no bias due to analyzing a lens system; the source quasar in 0957+561A/B is essentially a randomly chosen (by nature) object. Note, however, that 0957+561 is a radio-loud quasar and thus not an entirely fair test of the SB model. (In this context, we do not preclude the presence of a black hole in our SB model, since otherwise the radio emission of 0957+561 cannot be accounted for.) Nevertheless, we confine the present analysis to this best available data set but note that no firm conclusions can be achieved until good quality light curves are available for a statistically valid sample of AGNs.

The descriptions of models and structure functions including the numerical results are given in § 2. In § 3 we describe the time asymmetry in the observed and predicted light curves, and § 4 is devoted to discussion. Finally, we summarize our conclusions in § 5.

2. LIGHT CURVES AND STRUCTURE FUNCTION

2.1. *Structure Function Analysis*

Here we use only the first-order structure function described below. The general definition of structure functions and some of their properties are given by Simonetti et al. (1985). For a time series of optical magnitude $[m_{\rm opt}(t_i), i = 1, 2, \ldots; t_i < t_j]$, the first-order structure function, $V(\tau)$, and the autocorrelation function, $C(\tau)$, are defined as

$$V(\tau) \equiv \frac{1}{N(\tau)} \sum_{i<j} [m_{\rm opt}(t_i) - m_{\rm opt}(t_j)]^2 \quad (1)$$

$$C(\tau) \equiv \frac{1}{N(\tau)} \sum_{i<j} m_{\rm opt}(t_i) \times m_{\rm opt}(t_j) \, . \quad (2)$$

Summation is made over all pairs (i, j) for which $t_j - t_i = \tau$, and $N(\tau)$ denotes the number of such pairs. For a stationary random process the structure function is related to its autocorrelation function by

$$V(\tau) = 2[C(0) - C(\tau)] \, . \quad (3)$$

The typical shape of the measured structure functions basically consists of three distinct parts (cf. Hughes et al. 1992). First, there is a plateau at time lags longer than the longest correlation timescale, with a value of twice the variance of the fluctuations. Second, there is another plateau at short time lags, with a value corresponding to twice the variance of the measurement noise (which is absent in model calculations). Finally, the intermediate part between the two plateaus exhibits a power-law increase with increasing time lag:

$$[V(\tau)]^{1/2} \propto \tau^{\beta} \, . \quad (4)$$

In fact, the structure functions for the optical light curves of many AGNs increase steadily for $\tau \lesssim 2$–3 yr and flatten at larger lags (Hook et al. 1994; Trèvese et al. 1994; Cristiani et al. 1996; Cid Fernandes, Terlevich, & Aretxaga 1997). Its logarithmic slope (β) depends on the nature of the intrinsic variation of the source (e.g., shot noise, flicker noise, and so on). Kundić et al. (1997) report the results of photometric monitoring of 0957+561 A/B during about two years. The light curve and structure function of their data set are displayed in Figure 1, where $[V(\tau)]^{1/2}$ is calculated by averaging the structure functions of image A and B for each time lag τ. In Figure 1, $[V(\tau)]^{1/2}$ shows a logarithmic slope of $\beta \sim 0.35$ at $2 \lesssim \tau \lesssim 500$ days. Independently, Press et al. (1992) previously calculated the structure function for the same object based on the data available at that time and derived the logarithmic slope to be $\beta \sim 0.27$–0.34.

Although we do not know the logarithmic slopes of structure functions for optical light curves of a representative sample of AGN, the range of slopes β can be estimated by the slopes of power density spectra (PDS), using the relation between the structure function and PDS as follows: the typical PDS $[P(f)]$ is also described by a power law, $P(f) \propto f^{-\alpha}$, and the power-law index (α) is related to that of the structure function by $\alpha = 1 + 2\beta$ for $1 \leq \alpha \leq 3$, again under the condition that the time series is stationary (Hughes et al. 1992). For example, we have $\beta \sim 0.25$–0.40

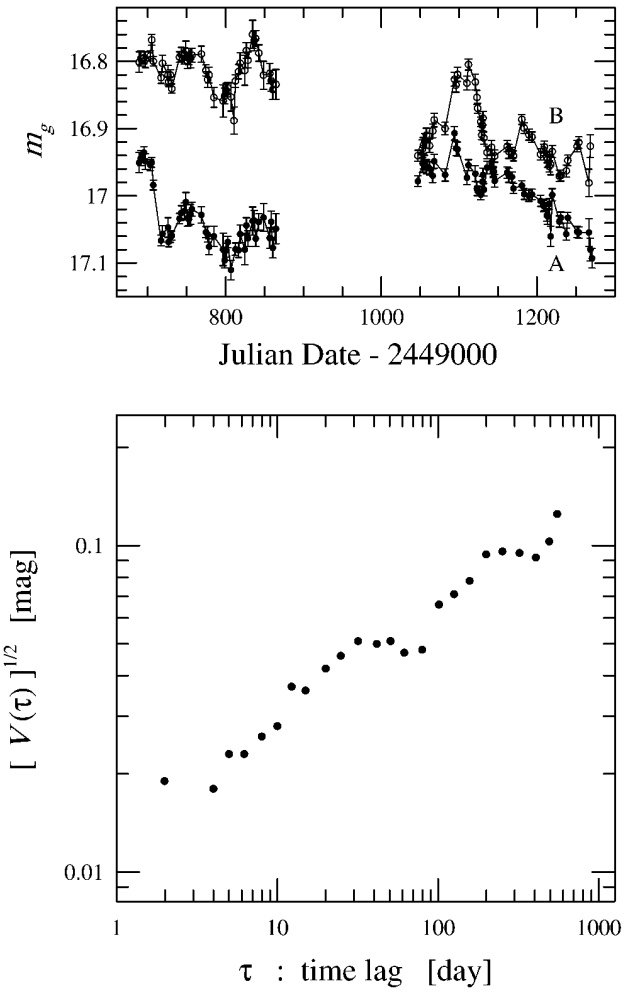

FIG. 1.—Light curve and structure function of 0957+561 calculated from the observational data by Kundić et al. (1997).

for $\alpha \sim 1.5$–1.8 (Lawrence & Papadakis 1993; see Hayashida et al. 1998 for X-ray variability data). If a given time series is produced by multiple superposition of some canonical shot (with a fixed time profile) at a random time, the analyzed values of β and α are determined solely by the profile of the canonical shot (see also Aretxaga, Cid Fernandes, & Terlevich 1997; Press & Rybicki 1997). If the frequency of shots depends on their magnitudes (e.g., small shots are frequent, whereas large shots are rare), the resultant PDS and structure function are influenced by the distribution of the size (peak intensity and duration) of individual shots (see Press 1978; Takeuchi, Mineshige, & Negoro 1995).

Incidentally, the time dilation effect due to cosmological redshifts may affect the estimations of timescale but does not influence on the logarithmic slopes of structure functions.

2.2. *The Starburst Model*

The starburst model (SB model) has been proposed in order to explain the properties of radio-quiet AGN, such as broad emission lines and optical variability (Terlevich et al. 1992; Aretxaga & Terlevich 1993; Cid Fernandes et al. 1997). According to this model, the optical variability of AGNs can be understood as the superposition of SNe distributed in a Poissonian way (Aretxaga & Terlevich 1994; Aretxaga 1997; Aretxaga et al. 1997). In this study, we calculate a fluctuation light curve, following Aretxaga et al. (1997). The generated variability is characterized by the following four parameters: (1) the background luminosity in the B -band due to stars, $L_{B_{\rm star}}$(in $L_{B_\odot}$); (2) the time after which radiative cooling becomes important in the evolution of the compact supernova remnants (cSNRs; see also Terlevich et al. 1992), $t_{\rm sg}$ (in days); (3) the energy released in the B-band by one event, ϵ_B ($\times 10^{51}$ ergs); and (4) the supernova rate; $\nu_{\rm SN}$ (yr^{-1}).

The basic element of the light variation is generated by a SN and the evolution of its associated cSNR. The shape of luminosity evolution in the B -band by a single event, $l(t)$, is thus determined by the superposition of that of a supernova, $l_{\rm SN}$, and that of its cSNR, $l_{\rm cSNR}(t)$, where

$$l_{\rm SN}(t) = \begin{cases} 0 & \text{for } t < 0 \\ 6 \times 10^9 \left(1 - \dfrac{t}{110}\right) L_{B_\odot} & \text{for } 0 \le t \le 110 \end{cases} \quad (5)$$

and

$$l_{\rm cSNR}(t) = \begin{cases} 3 \times 10^{10}\, \dfrac{365\epsilon_B}{t_{\rm sg}} \left(\dfrac{t - 0.3t_{\rm sg}}{0.7t_{\rm sg}}\right) L_{B_\odot} & \text{for } 0.3t_{\rm sg} \le t \le t_{\rm sg} \\ 3 \times 10^{10}\, \dfrac{365\epsilon_B}{t_{\rm sg}} \left(\dfrac{t}{t_{\rm sg}}\right)^{-11/7} L_{B_\odot} & \text{for } t_{\rm sg} \le t\ . \end{cases} \quad (6)$$

Therefore, the first peak (at $t = 0$) is due to a SN, while the second one (at $t = t_{\rm sg}$) is due to its cSNR, respectively. An example of $l(t)$ plotted in Figure 2, shows a sudden rise and a gradual decay. Here, we use $t_{\rm sg} = 280$ days and $\epsilon_B = 0.5$ ($\times 10^{51}$ ergs).

There are constraints on the four parameters from the observations. First, since both the SN rate ($\nu_{\rm SN}$) and the B -band luminosity coming from stars ($L_{B_{\rm star}}$) are linked to the

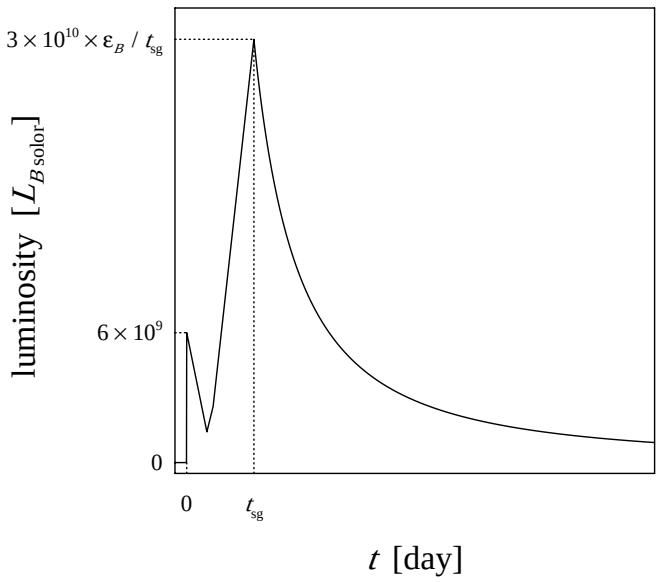

FIG. 2.—Typical light curve of one shot in the starburst model for $t_{\rm sg} = 280$ days and $\epsilon_B = 0.5 \times 10^{51}$ ergs. The first peak (at $t = 0$) is due to a SN, and the second peak (at $t = t_{\rm sg}$) is caused by a subsequent cSNR. The light variation is time asymmetric; rapid rise and gradual decay are shown.

number of massive stars, the ratio of $\nu_{\rm SN}$ to $L_{B_{\rm star}}$ is approximately given by the expression (Aretxaga & Terlevich 1994)

$$\frac{\nu_{\rm SN}}{L_{B_{\rm star}}} \approx 2 \times 10^{-11}\ {\rm yr}^{-1}\ L_{B_\odot}^{-1}\ . \tag{7}$$

Second, the cooling timescale of the cSNRs ($t_{\rm sg}$) was found to be $\sim$260–280 days from the observations of NGC 4151 and NGC 5548 (Aretxaga & Terlevich 1993, 1994), while for QSOs, which may have higher metallicities (Hamann & Ferland 1992, 1993), the cooling timescale could be shorter. Therefore, we adopt $t_{\rm sg} \lesssim 280$ days in numerical calculations. Third, an estimation of ϵ_B can be obtained from the observed time-averaged equivalent width of Hβ (for details, see Aretxaga & Terlevich 1994),

$$\overline{W_{\rm H\beta}} \sim 320\ \frac{\epsilon_B}{1 + 0.17\epsilon_B}\ \text{Å}\ . \tag{8}$$

With the observed equivalent width of Hβ in QSOs, $\overline{W_{\rm H\beta}} \sim$ 100Å (Osterbrock 1991), ϵ_B is estimated to be $\epsilon_B \sim 0.5 \times 10^{51}$ ergs. For the fourth parameter, the SN rate ($\nu_{\rm SN}$) is linked to the time average of the total B-band luminosity of the individual AGN ($\overline{L_{B_T}}$) according to equation (7) by

$$\begin{aligned}\overline{L_{B_T}} &= L_{B_{\rm star}} L_{B_\odot} + \epsilon_B \nu_{\rm SN} \times 10^{51}\ {\rm ergs\ yr}^{-1} \\ &\approx 5 \times 10^{10} \nu_{\rm SN}(1 + \epsilon_B) L_{B_\odot}\ .\end{aligned} \tag{9}$$

To construct simulated AGN light curves based on this model, we superposed SN + cSNR light curves of a given $t_{\rm sg}$ at a random time with a rate $\nu_{\rm SN}$. The value of $\nu_{\rm SN}$ determines the event rate and the luminosity coming from stars in equation (7), while the value of $t_{\rm sg}$ determines the cooling timescale and the peak luminosity of cSNR. Each event may have slightly different cooling timescales ($t_{\rm sg}$) and released energies (ϵ_B) around mean values. To consider this issue, we assumed that the values of $t_{\rm sg}$ and ϵ_B vary in a Gaussian way around their mean, such that factor of 2 variation corresponds to twice the value of the standard deviation of a Gaussian distribution (see Aretxaga et al. 1997).

We performed Monte Carlo simulations based on the SB model described above to calculate light curves and structure functions. We focused our attention on the slope of the structure function, β, since this is a key diagnostic to distinguish between the SB model and the DI model. Figure 3 shows an example of the results: the upper two panels represent light curves with different parameter sets, and the bottom panel shows the $[V(\tau)]^{1/2}$ of these light curves with a total time of 8×10^4 days. The structure function produced by this model increases in a power law $\{[V(\tau)]^{1/2} \propto \tau^\beta\}$ with a logarithmic slope of $\sim$0.74–0.90 at $\tau \lesssim t_{\rm sg}$ depending on the parameters (see Table 1), and flattens at the time scale, $t_{\rm sg}$. The results of all the calculated SB models are summarized in Table 1. There is a clear tendency that the slope of the structure function depends only on the shape of each shot (i.e., $t_{\rm sg}$) and not on the event rate (i.e., $\nu_{\rm SN}$). This agrees with the theoretical expectation (see § 2.1).

Incidentally, 0957 + 561, which we adopted for comparison with the models, corresponds to $\nu_{\rm SN} \sim 50\ {\rm yr}^{-1}$, assuming $M_B \sim -26$. The observed light curve yields a more gradual slope of the structure function, $\beta \sim 0.35$ (Fig. 1), which is too small to account for solely in terms of starbursts. However, there exists a possibility that thermal instabilities in cSNRs (see, e.g., Plewa 1995), which are neglected in the present analytical approximation (eqs. [5] and [6]), may produce a highly variable light curve over weeks to months above the light curve calculated by the approximation (see Cid Fernandes et al. 1996). If this is the case, the resultant slopes for the SB model may change significantly (R. Terlevich & I. Aretxaga 1998, private communication).

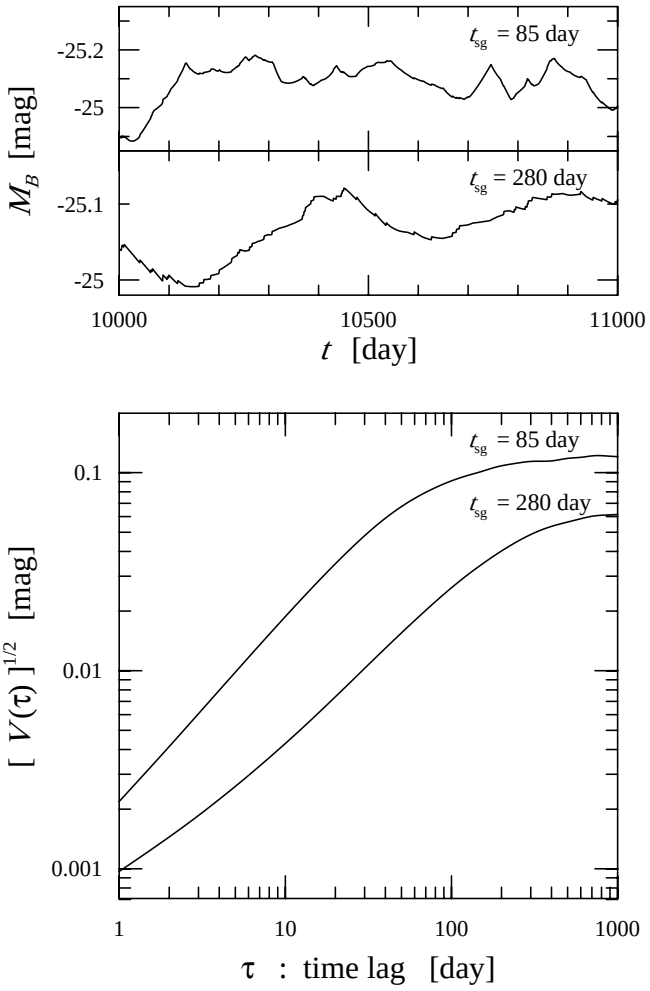

FIG. 3.—Example of the light curves (*upper two panels*) and the structure functions (*bottom panel*) produced by the starburst model. In this figure, the rate of SNe $\nu_{\rm SN} = 20\ {\rm yr}^{-1}$, and $t_{\rm sg}$ (the cooling timescales of cSNRs) is labeled inside each panel. The structure functions $\{[V(\tau)]^{1/2}\}$ grow in a power-law way ($[V(\tau)]^{1/2} \propto \tau^\beta$) at small τ.

TABLE 1

SLOPES OF THE STRUCTURE FUNCTION, β, FOR THE STARBURST MODEL

$\nu_{\rm SN}$ (yr^{-1})	$t_{\rm sg}$ (days)		
	85	180	280
5	0.90	0.82	0.74
20	0.90	0.83	0.74
100	0.90	0.83	0.74

NOTE.—We assumed $[V(\tau)]^{1/2} \propto \tau^\beta$. Here, $\nu_{\rm SN}$ is the supernova rate and $t_{\rm sg}$ represents the cooling timescale of the cSNR. Since the second parameter, $t_{\rm sg}$, actually controls the shape of one shot, resultant slopes of structure functions depend solely on $t_{\rm sg}$ (see § 2.1).

2.3. *The Cellular-Automaton Model for the Disk Instability*

For the disk-instability model, we consider an accretion-disk atmosphere emitting a power-law X-ray spectrum that is substantially fluctuating in time. Our hypothesis for generating the optical fluctuation is that some instability taking place in the atmosphere leads to the optical variability. According to this hypothesis, we adopt the cellular-automaton model (Mineshige, Ouchi, & Nishimori 1994). The resultant light curves and PDS produced by the model are in good agreement with those of the observed fluctuations. We pursue their calculation methods to produce fluctuating light curves in the optical band, assuming that the optical variability simply follows the X-ray variability with little delay.

The procedure to calculate fluctuations is as follows (see Takeuchi et al. 1995).

1. We divide the disk plane into numerous cells along the two-dimensional circular coordinates (r, φ). Each cell is thus characterized by two coordinates, $r_i (i = 1 - I)$ and $\varphi_j (j = 1 - J)$. A larger i means a smaller radius ($r_{i+1} < r_i$).
2. After choosing one cell randomly at the outermost ring (i.e., $i = 1$), we put a gas particle with a mass m into the selected cell. This process represents a mass supply to the disk that rotates around a supermassive black hole.
3. We choose one cell at each ring randomly and let a small amount of mass, $m' \ll m$, fall into the adjacent inner cell with same φ. This process corresponds to gradual viscous diffusion and is needed to reproduce the observed properties.
4. For unstable cells, where the mass density exceeds a critical value that is given a priori, we let 3 mass particles fall from that cell equally into three adjacent cells at the adjacent inner ring. In other words, if the mass density at (r_i, φ_j) exceeds a critical value [i.e., $M_{i,j} > M_{\rm crit}(r_i)$], we set

$$\begin{aligned} M_{i,j} &\rightarrow M_{i,j} - 3m \,, \\ M_{i+1,j\pm1} &\rightarrow M_{i+1,j\pm1} + m \,, \\ M_{i+1,j} &\rightarrow M_{i+1,j} + m \,. \end{aligned} \tag{10}$$

This process corresponds to an avalanche flow or a flare. The inner cells may become unstable as the result of an avalanche flow from above. In that case, a subsequent avalanche flow can occur in a next time step (after repeating procedures 2 and 3, above).
5. We repeat processes 2–4 over 10^4 times to remove the effect of the initial condition and minimize statistical errors. Each mass blob can travel over 1 mesh point at maximum within 1 time step. Figure 4 shows a schematic view of those procedures.

It is known (Bak, Tang, & Wiesenfeld 1988) that under such circumstances, the disk automaton will evolve to and stay at a self-organized critical state. In this state, most single flares calm down without triggering subsequent avalanches, but some single flares trigger small-scale avalanches over several radial mesh points. Furthermore, although quite rarely, it is possible for a single flare to trigger a large-scale avalanche involving almost the entire region. The mass density in each cell ($M_{i,j}$) always remains slightly lower than the critical mass density ($M_{\rm crit}$); thus the resultant light curve does not depend on the value of $M_{\rm crit}$. Here, we adopt the two-dimensional disk that undergoes a rigid rotation for simplicity, but it is easily demonstrated that even if three-dimensional structure of the disk (i.e., r-, φ-, and z-directions) and the effects of differential rotation are taken into account, the outcome will not change significantly (Takeuchi et al. 1995).

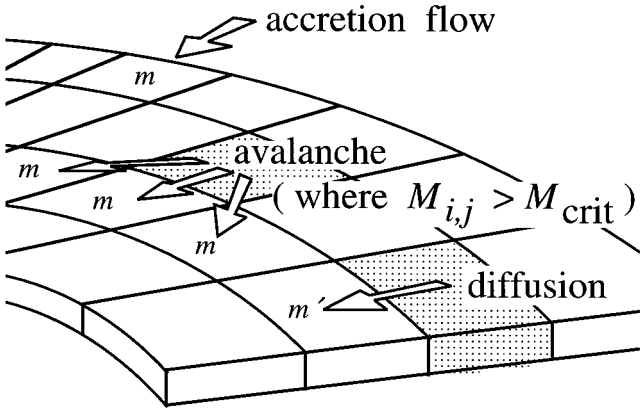

FIG. 4.—Schematic view of our cellular-automaton model

In the present DI model, the time step is not a priori specified. To give timescales, we must specify disk models that describe the dynamical behavior of atmosphere. For example, if we relate this model to the advection-dominated accretion flow (ADAF) model (Abramowicz et al. 1995; Narayan & Yi 1995; Manmoto, Mineshige, & Kusunose 1997), the characteristic timescale in the light curve corresponds to the accretion timescale, $\tau_{\rm acc}$, from $r_{\rm out}$ to $r_{\rm in}$ (Manmoto et al. 1996). The radial velocity of the ADAF model is less than or comparable to the free-fall velocity, though that of the standard accretion disk model is much less. Thus we approximately estimate the timescale ($\tau_{\rm acc}$) for the ADAF as

$$\tau_{\rm acc} \gtrsim \left(\frac{r^3}{GM}\right)^{1/2} = 160\left(\frac{r}{10^2 r_g}\right)^{3/2}\left(\frac{M}{10^9\, M_\odot}\right) \text{ days} \,, \tag{11}$$

where r_g is Schwarzschild radius defined by

$$r_g \equiv \frac{2GM}{c^2} \,. \tag{12}$$

We performed Monte Carlo simulations for several parameter sets, following the cellular-automaton procedure. Examples of the calculated light curves and structure functions with a total time step of 8×10^4 are shown in Figure 5. The model parameters are shown in Table 2; here, $m' = 0.1m$, means that the ratio of diffusion mass to inflow

TABLE 2

SLOPES OF THE STRUCTURE FUNCTION, β, FOR THE DISK-INSTABILITY MODEL

	m'/m		
$r_{\rm in}:r_{\rm out}$	0.02	0.1	0.5
1:4	0.49	0.46	0.44
1:20	0.43	0.42	0.41
1:100.....	0.42	0.42	0.41

NOTE.—Here, $m' = 0.1m$ means that the ratio of diffusion mass to inflow mass is 0.1, and $r_{\rm in}$ and $r_{\rm out}$ denote the inner radius and the outer radii, respectively, of the calculated disk region.

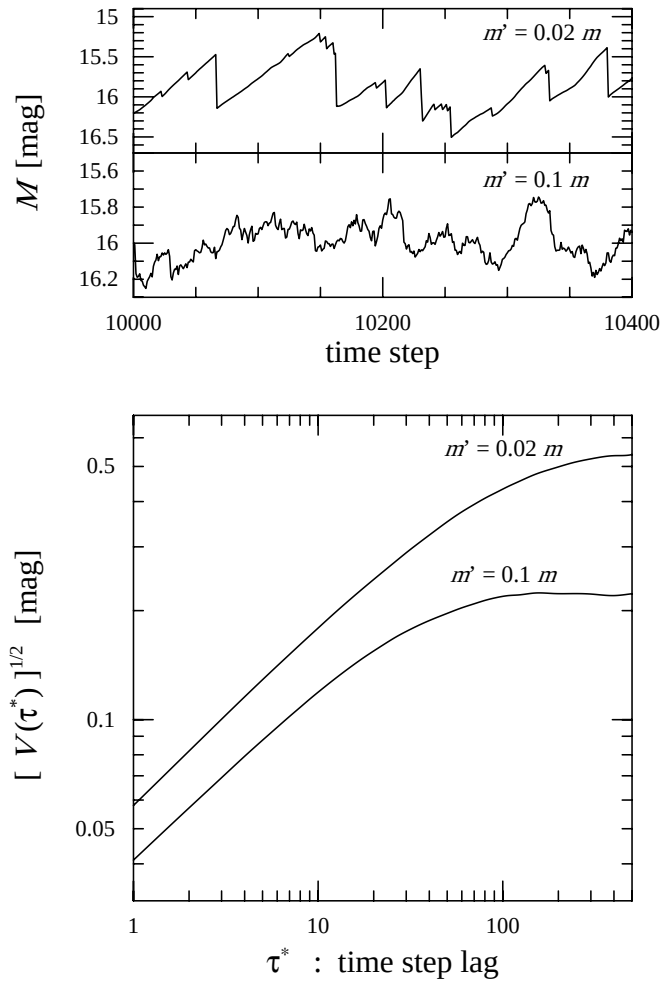

FIG. 5.—Same as Fig. 3 but for our cellular-automaton model for the disk instability. Here, the ratio of inner edge to outer edge of the disk $r_{in}:r_{out} = 1:20$ and m'/m (the ratio of diffusion mass to inflow mass) is labeled in each panel.

mass is 0.1, and r_{in} and r_{out} represent the inner radius and outer radius of the calculated disk region, respectively. In this model, we found that each $[V(\tau)]^{1/2}$ increases in a power-law fashion, $[V(\tau)]^{1/2} \propto \tau^{\beta}$, at $\tau \lesssim \tau_{acc}$ and flattens at the timescale, τ_{acc}, as we have seen in the starburst model, but the logarithmic slopes are systematically smaller than those of the SB model: $\beta \sim 0.41$–0.49 (see Table 2), with rather weak dependence on the parameters. These values are closer to the observed ones. In the present DI model, the resultant logarithmic slopes seem to depend both on the characteristic luminosity profile of a largest scale avalanche and on the distribution of avalanches with different scales (§ 2.1).

We do not include relativistic effects in the present DI model. However, such effects are substantial only for gas blobs near the central massive black hole, where the dynamical timescale τ_{dyn} is

$$\tau_{dyn} \sim \left(\frac{r^3}{GM}\right)^{1/2} \sim 0.8\left(\frac{r}{3r_g}\right)^{3/2}\left(\frac{M}{10^9\ M_\odot}\right) \text{ day} .$$

Hence they may affect structure functions for $\tau \lesssim 1$ day, but they cannot substantially change the overall shape for $\tau > 1$ day. Consequently, we can conclude that the DI model is favored over the SB model in explaining a well-observed AGN light curve, which has the structure function slope of $\beta \sim 0.35$.

3. ANALYSIS OF TIME ASYMMETRY

Two-point statistics (correlation function, structure function, or power spectrum) cannot define an arrow of time from data sets. Thus, whether the light curve favors rapid rise (and gradual decay) or gradual rise (and rapid decay) can in principle be measured by three-point statistical quantities. To examine such a deviation from time symmetry, Press & Rybicki (1997) simulated light curves by multiple superposition with some rate, ν, of a certain canonical shot that has a simple time-asymmetric profile. They analyzed and compared the light curves of 0957+561 and the simulated ones in terms of three-point statistics, concluding that simulated light curves with small ν have large time asymmetries, and consequently that the observed light curves rule out the models with rates of superposition (ν) that are less than 90 yr^{-1}.

To evaluate the time asymmetry of the light curve, we adopt an alternative approach: we separate $V(\tau)$ into two parts, $V_+(\tau)$ and $V_-(\tau)$ (hereafter plus and minus structure functions, respectively), depending on the sign of $m_{opt}(t_i) - m_{opt}(t_j)$:

$$V_+(\tau) \equiv \frac{1}{N_+(\tau)} \sum_{i<j} [m_{opt}(t_i) - m_{opt}(t_j)]^2 \quad \text{for} \quad m_{opt}(t_i) - m_{opt}(t_j) > 0 , \quad (13)$$

$$V_-(\tau) \equiv \frac{1}{N_-(\tau)} \sum_{i<j} [m_{opt}(t_i) - m_{opt}(t_j)]^2 \quad \text{for} \quad m_{opt}(t_i) - m_{opt}(t_j) < 0 , \quad (14)$$

where the summations in the expressions of $V_+(\tau)$ and $V_-(\tau)$ are made, respectively, only for pairs that have plus and minus signs of $m_{opt}(t_i) - m_{opt}(t_j)$, and $N_+(\tau)$ and $N_-(\tau)$ are the numbers of such pairs. Decreasing $m(t_i)$ with time, i.e., $m_{opt}(t_i) - m_{opt}(t_j) > 0$, represents increasing luminosity with time; thus $V_+(\tau)$ approximately indicates the structure function of brightening phases, and, similarly, $V_-(\tau)$ roughly expresses that of decaying phases.

If the data is produced by time-symmetric processes, $V_+(\tau)$ and $V_-(\tau)$ are expected to coincide with $V(\tau)$. On the other hand, a significant discrepancy would indicate a deviation from time symmetry; for example, $V_+(\tau) \gtrsim V_-(\tau)$ means that the light curve favors a rapid rise and gradual decay.

Figure 6 displays the plus and minus structure functions, $V_+(\tau)$ and $V_-(\tau)$ (*top panels*) and the relative difference between them, $[V_+(\tau)]^{1/2} - [V_-(\tau)]^{1/2}$, normalized by the usual structure function $[V(\tau)]^{1/2}$ (*bottom panels*) for the SB model with several parameter sets. Figure 6*a* shows the case for $t_{sg} = 85$ days and Figure 6*b* is for $t_{sg} = 280$ days. In both top panels, the plus and minus structure functions are represented by upward filled and downward open triangles, respectively, while the solid lines in all panels represent the cases of $\nu_{SN} = 5$, 20, and 100 yr^{-1}, from the top to the bottom, respectively. The error bars in the bottom panels are calculated providing that the uncertainty of $[V_+(\tau)]^{1/2} - [V_-(\tau)]^{1/2}$ approximately equals to $2^{1/2}$ times the errors in the photometry ($\sim \pm 0.011$ mag). All the results show time asymmetry to some extent; there is a signature of rapid rise and slow decline, as expected from the single-event

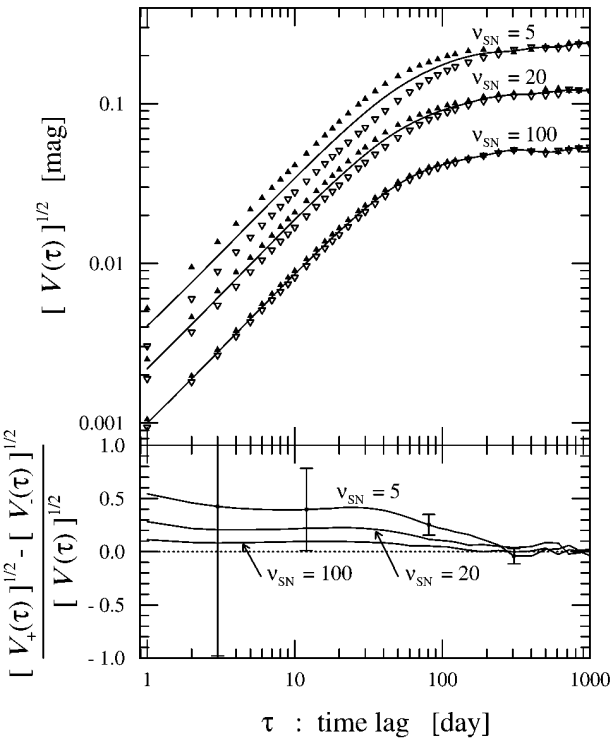

FIG. 6a

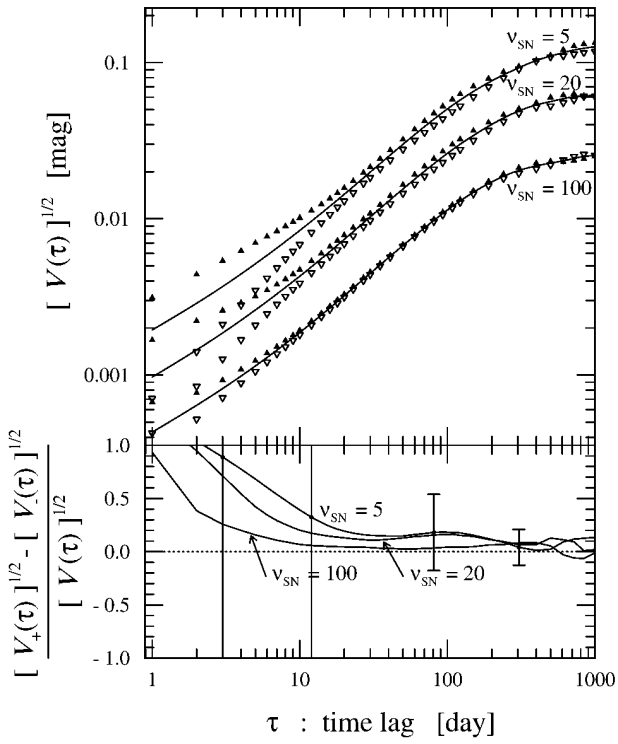

FIG. 6b

FIG. 6.—Time asymmetry calculated in terms of the plus and minus structure functions, $[V_+(\tau)]^{1/2}$ and $[V_-(\tau)]^{1/2}$, for the SB model with (*a*) $t_{sg} = 85$ days and with (*b*) $t_{sg} = 280$ days, respectively. *Top panels*: The usual structure functions are shown by the solid lines, while the plus and minus structure functions are indicated by upward-pointing filled and downward-pointing open triangles, respectively. See eqs. (13) and (14) for their definitions. The models show time asymmetry to some extent in the sense of a rapid rise and a slow decline. *Bottom panels*: The relative differences between $[V_+(\tau)]^{1/2}$ and $[V_-(\tau)]^{1/2}$ normalized by $[V(\tau)]^{1/2}$ are depicted.

profile (Fig. 2). As pointed out by Press & Rybicki (1997), there is a trend that the smaller ν_{SN} is, the larger the resulting time asymmetry in the SB model. Within errors in the photometry, both $V_+(\tau)$ and $V_-(\tau)$ are consistent with time symmetry except for the models with $\nu_{SN} \lesssim 10$ yr^{-1}, which shows a significant discrepancy at $\tau \lesssim 100$ days.

We also calculated the plus and minus structure functions for the DI model, which are depicted in Figure 7. Here the solid lines in the bottom panel represent the cases of $m' = 0.5m$, $0.1m$, and $0.02m$, from the top to the bottom, respectively. In contrast to the SB model, the relative difference between them shows the signature of a gradual rise and a rapid decay, and, moreover, the tendency becomes enhanced in the case of $m' \lesssim 0.1m$. This time asymmetry comes from the shape of the luminosity variation due to a single large-scale avalanche. An avalanche flow starting at some outer radius leads to luminosity variation over an accretion timescale, τ_{acc}, in which the emissivity increases as the flow approaches the center. Thus the light curve shows a gradual brightening over τ_{acc}. After the front of the flow reaches the innermost region, the amount of radiation rapidly decays; this is responsible for the rapid decline in the light curve (see, however, § 4 for hydrodynamic effects). However, a large m' causes frequent small-scale avalanches, which hide the time asymmetry.

Finally, Figure 8 displays $V_+(\tau)$ and $V_-(\tau)$ and their relative differences for the observed light curve of 0957+561. The bottom panel of the figure shows the relative differences fluctuating at $\tau \gtrsim 70$ days, which can be ascribed to the effect of the finite length of the observational light curve. Thus we focus our attention solely to the differences at $\tau \lesssim 70$ days. In this range of time lags τ, apparent time asymmetry appears in the sense of a slow rise and a rapid decline, but it is premature to conclude that this tendency is real. This is because photometric monitoring over two years is still too short to calculate reliable three-point statistics. Longer observational data sets will be valuable for this purpose (see also Press & Rybicki 1997). Further, estimating time asymmetry from longer observations will pose effective constraints on models even if they possess similar logarithmic slopes in the structure functions.

4. DISCUSSION

We have compared two models, DI and SB, to see how well the statistical properties of the best available AGN optical light curve can be understood. In this section, we will discuss several related issues.

The first issue concerns the time asymmetry in simulated light curves based on the two models. Light curves in the DI model obtained by the present cellular-automaton simulations show an apparent time asymmetry with slow rise and rapid decline under the condition $m' \lesssim 0.1m$. This is because each shot profile obtained by the model possesses a time asymmetry and this becomes more enhanced in the case of smaller m', as we mentioned above. We should be, however, careful about this result, since the cellular-automaton simulations neglect hydrodynamic effects. According to the one-dimensional, hydrodynamic simulations of X-ray fluctuations from black hole objects by Manmoto et al. (1996), an individual shot has a rather time-symmetric profile due to wave reflection (see also Takeuchi & Mineshige 1997). Such hydrodynamic effects as wave reflection

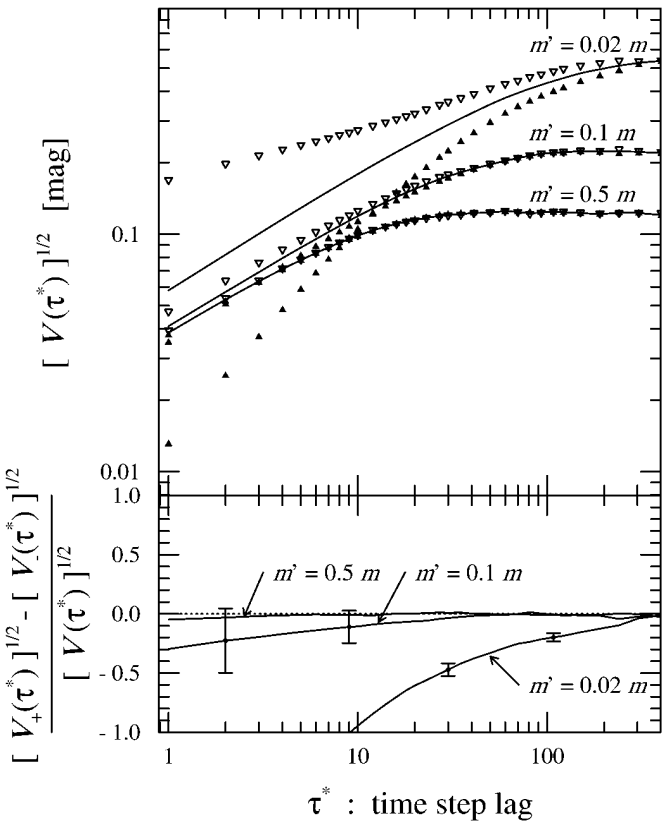

FIG. 7.—Same as Fig. 6 but for the DI model with $m'/m = 0.02$, 0.1, and 0.5. The ratio of the outer to inner disk radii is fixed to be $r_{out}/r_{in} = 20$. The models show some time asymmetry in the sense of a slow rise and a rapid decline.

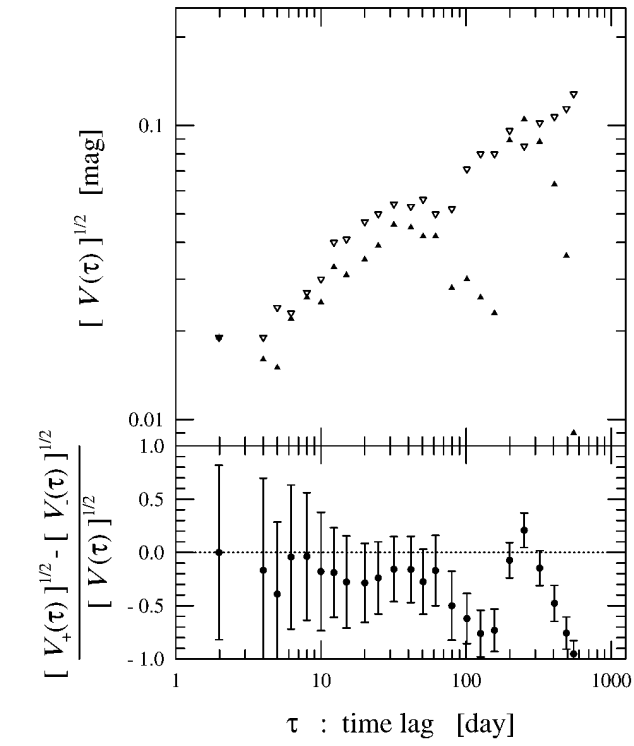

FIG. 8.—Plus and minus structure functions calculated from the observations of 0957+561, corresponding to Figs. 6 and 7. There is a hint of a tendency for a slow rise and a rapid decay.

are not included in the present simulations. If they are included, the light curves would show more time symmetry. The SB model, on the other hand, predicts clear time asymmetry (rapid rise and slow decline), unless $\nu_{SN} \gtrsim 10\ \mathrm{yr}^{-1}$. In the context of the SB model such a high supernova rate implies objects of larger luminosity such as QSOs; thus, time asymmetry of such luminous AGNs might be hidden by observational errors.

Second, we consider the wavelength dependence of the timescales of AGN optical variability. There is a discussion of the origin of AGN long-term variability initiated by Hawkins (1993), who has claimed that gravitational microlensing can account for the absence of the expected time-dilation effect in the observations of high-redshift quasars. Alternatively, Baganoff & Malkan (1995) have suggested that the relatively hot region of a standard accretion disk radiating at shorter wavelengths should be restricted to the inner region. Thus, when we observe objects with higher redshifts, we detect radiation of shorter wavelengths in the rest frame, i.e., those coming from the inner part, where temperatures are higher and dynamical timescales are shorter. This roughly cancels out the expected time-dilation effect. Hawkins & Taylor (1997), however, argue that the standard accretion disk model predicts wavelength-dependent variability timescales as stated in Baganoff & Malkan (1995) and that the prediction is inconsistent with observations of the quasar sample and of NGC 5548. They conclude that microlensing is preferable as an explanation for quasar variability, although the nearby Seyfert galaxies probably show intrinsic variations.

In relation to this issue, we can make two points. Contrary to the claim by Hawkins & Taylor (1997), microlensing of an optically thick standard accretion disk produces wavelength-dependent time variations (Yonehara et al. 1997a). Furthermore, if occasional avalanche flows occur at various radii, as we have found in the cellular automata DI model, wavelength-independent variation timescales are produced naturally (Yonehara, Mineshige, & Welsh 1997b). Third, we discuss the amplitudes of the luminosity variations as a function of wavelength. Multiwavelength observations of AGNs have revealed that the variation amplitude in optical-ultraviolet bands is larger at shorter wavelengths (Di Clemente et al. 1996; Edelson et al. 1996). This suggests that the outer cool region of the disk, emitting at longer wavelengths, is less variable than the inner hot region, emitting at shorter wavelengths. This tendency could also be understood in our DI model, since an avalanche flow starting at the outer region drifts down, spreading the avalanche region (see also Yonehara et al. 1997a) to a larger fraction of the inner region.

Fourth, we briefly comment on the relation between X-ray variability of AGNs and that of X-ray binaries (XBs). X-rays from AGNs and XBs are known to behave in similar manners and to exhibit similar shapes of PDS and similar shotlike features in their light curves. This similarity strongly suggests a common mechanism being responsible for the X-ray variability of both types of objects. It is obvious that XB variability cannot be explained by microlensing or starburst models, but there is certainly evidence that it is associated with an accretion disk. If AGN variability and XB variability do have the same origin, as is strongly suggested by their similar statistical properties (Hayashida et al. 1998), AGN variability is also likely to be of accretion-disk origin.

Finally, there still remains, of course, a possibility that

AGN variability is caused by several independent mechanisms. The composite effects of the different variability mechanisms on the structure functions may be investigated in the future.

5. CONCLUSION

We have calculated the structure functions $V(\tau)$ for simulated light curves of the two models and the observed $0957+561$ light curve to determine which model provides a better match.

1. We summarize the values of the logarithmic slopes β of $V(\tau)$ among the two models and the observation; $\beta \sim 0.74$–0.90 in the SB model and $\beta \sim 0.41$–0.49 in the DI model, while the observed light curve exhibits $\beta \sim 0.35$. Therefore we may conclude the DI model is preferable to the SB model in accounting for the observed value of β in the case of $0957+561$. There exists, however, a possibility that the SB model might yield a more gradual slope if thermal instabilities in supernova remnants were incorporated.

2. The two models exhibit opposite trends of time asymmetry, though the size of the deviations from time symmetry depend on the model parameters. Thus, the time asymmetry in the light curves potentially offer effective information to test the models. However, the presently available observational data sets do not allow us to make use of this diagnostic. Thus, we must await longer duration observational light curves.

We acknowledge Roberto Terlevich and Itziar Aretxaga for valuable comments on the starburst model, and the anonymous referee for criticisms that helped improve the paper. One of the authors (T. K.) wishes to thank Karen M. Leighly for useful discussions regarding time series analysis. He also thanks Tsutomu T. Takeuchi, Atsunori Yonehara, and Hiroyuki Hirashita for helpful comments and encouragement. This work was supported in part by the Japan-US Cooperative Research Program, which is funded by the Japan Society for the Promotion of Science and the US National Science Foundation, and by the Grants-in-Aid of the Ministry of Education, Science, and Culture of Japan, 08640329, 09223212 (S. M.).

REFERENCES

Abramowicz, M. A., Chen, X., Kato, S., Lasota, J. -P., & Regev, O. 1995, ApJ, 438, L37
Aretxaga, I. 1997, Rev. Mexicana Astron. Astrofis., 6, 207
Aretxaga, I., Cid Fernandes, R., & Terlevich R. J. 1997, MNRAS, 286, 271
Aretxaga, I., & Terlevich, R. 1993, Ap&SS, 205, 69
———. 1994, MNRAS, 269, 462
Baganoff, F. K., & Malkan, M. A. 1995, ApJ, 444, L13
Bak, P., Tang C., & Wiesenfeld, K. 1988, Phys. Rev. A, 38, 364
Cid Fernandes, R., Plewa, T., Różyczka, M., Franco, J., Terlevich, R., Tenorio-Tagle, G., & Miller, W. 1996, MNRAS, 283, 419
Cid Fernandes, R., Terlevich, R., & Aretxaga, I. 1997, MNRAS, 289, 318
Clavel, J. C., et al. 1992, ApJ, 393, 113
Cristiani, S., Trentini, S., La Franca, F., Aretxaga, I., Andreani, P., Vio, R., & Gemmoo, A. 1996, A&A, 306, 395
Di Clemente, A., Giallongo, E., Natali, G., Trèvese, D., & Vagnetti, F. 1996, ApJ, 463, 466
Edelson, R. A., et al. 1996, ApJ, 470, 364
Green, A. R., McHardy, I. M., & Lehto, H. J. 1993, MNRAS, 265, 664
Haarsma, D. B., Hewitt, J. N., Lehar, J., & Burke, B. F. 1997, 479, 102
Hamann, F., & Ferland, G. 1992, ApJ, 391, L53
———. 1993, ApJ, 418, 11
Hawkins, M. R. S. 1993, Nature, 366, 242
Hawkins, M. R. S., & Taylor, A. N. 1997, ApJ, 482, L5
Hayashida, K., Miyamoto, S., Kitamoto, S., Negoro, H., & Inoue, H. 1998, ApJ, 500, 642
Hughes, P. A., Aller, H. D., & Aller, M. F. 1992, ApJ, 396, 469
Hook, I. M., McMahon, R. G., Boyle, B. J., & Irwin, M. J. 1994, MNRAS, 268, 305
Krolik, J. H., Kallman, T. R., Malkan, M. A., Edelson, R. A., & Kriss, G. A. 1991, ApJ, 371, 541
Kundić, T., et al. 1995, ApJ, 455, L5
———. 1997, ApJ, 482, 75
Lawrence, A., & Papadakis, I. 1993, ApJ, 414, L85
Leighly, K. M., & O'Brien, P. T. 1997, ApJ, 481, L15
Malkan, M. A. 1983, ApJ, 268, 582
Manmoto, T., Mineshige, S., & Kusunose, M. 1997, ApJ, 489, 791
Manmoto, T., Takeuchi, M., Mineshige, S., Matsumoto, R., and Negoro, H. 1996, ApJ, 464, L135
Mineshige, S., Ouchi, B. N., & Nishimori, H. 1994, PASJ, 46, 97
Narayan, R., & Yi, I. 1995, ApJ, 452, 710
Netzer, H., & Peterson, B. M. 1997, in Astronomical Time Series, ed. D. Maoz, A. Stermberg, & E. M. Leibowitz (Dordrecht: Kluwer), 85
O'Brien, P. T., & Leighly, K. M. 1997, preprint (astro-ph 9701105)
Osterbrock, D. E. 1991, Rep. Prog. Phys., 54, 579
Peterson, B. M., et al. 1994, ApJ, 425, 622
Plewa, T. 1995, MNRAS, 275, 143
Press, W. H. 1978, Comments Astrophys., 7, 103
Press, W. H., & Rybicki, G. B. 1997, in Astronomical Time Series, ed. D. Maoz, A. Stermberg, and E. M. Leibowitz (Dordrecht: Kluwer), 61
Press, W. H., Rybicki, G. B., & Hewitt, J. N. 1992, ApJ, 385, 404
Rees, M. J. 1984, ARA&A, 22, 471
Santos-Lleó, M., Clavel, J., Barr, P., Glass, I. S., Pelat, P., Peterson, B. M., & Reichert, G. 1995, MNRAS, 274, 1
Shields, G. A. 1978, Nature, 272, 706
Simonetti, J. H., Cordes, J. M., & Heeschen, D. S. 1985, ApJ, 296, 46
Takeuchi, M., & Mineshige, S. 1997, ApJ, 486, 160
Takeuchi, M., Mineshige, S., & Negoro, H. 1995, PASJ, 47, 617
Tanaka, Y., et al. 1995, Nature, 375, 659
Terlevich, R., Tenorio-Tagle, G., Franco, J., & Melnick, J. 1992, MNRAS, 255, 713
Trèvese, D., Kron, R. G., Majewski, S. R., Bershady, M. A., & Koo, D. C. 1994, ApJ, 433, 494
Warwick, R. S., et al. 1996, ApJ, 470, 349
Yonehara, A., Mineshige, S., Fukue, J., Umemura, M., & Turner, E. L. 1997a, preprint (astro-ph 9710190)
Yonehara, A., Mineshige, S., & Welsh, W. F. 1997b, ApJ, 486, 388